Progress In Electromagnetics Research, PIER 82, 401–418, 2008

DESIGN OF COMPACT VIVALDI ANTENNA ARRAYS FOR UWB SEE THROUGH WALL APPLICATIONS

Y. Yang, Y. Wang, and A. E. Fathy

EECS Department
University of Tennessee
1508 Middle Drive, Knoxville, TN 37996, USA

Abstract—Two different types of Vivaldi antenna arrays have been designed for UWB see through wall applications. The first is a 16×1 antipodal Vivaldi antenna covering 8–12 GHz, and the second is an 8×1 tapered slot antenna for 2–4 GHz frequency range. The array elements are optimized to have a compact size and almost constant gain with frequency. Wilkinson power dividers were designed and fabricated to compose the feed network for the Vivaldi antenna arrays. Measured results of the manufactured antipodal and tapered slot Vivaldi antenna arrays are in excellent agreement with the simulated ones, with a gain of more than 13 dBi and 12 dBi respectively within their respective operating band. The first array is geared towards see through dry wall with high resolution, while the second is designed at lower frequencies to allow see through concrete wall applications. Full arrays were manufactured and connected to multi-throw switches and have been utilized as part of synthetic aperture radar.

1. INTRODUCTION

For See-Through-Wall (STW) application, the transmitting and receiving antennas must be compact and lightweight for portability. Besides the requirements on their physical size, the antenna must be able to transmit UWB pulses with minimal distortion [1, 2]. The antenna radiation pattern needs to be accounted for — since significant image distortion might be seen due to the radiation pattern angle dependence. Here we use Vivaldi antennas because of their favorable characteristics for STW application, and specifically they have relatively simple structure, light weight, small lateral dimensions, wideband, high efficiency, and high gain characteristics, they are excellent candidates for array applications. Theoretical and

experimental analysis of Vivaldi antenna characteristics can be found in [3–8]. Variants of Vivaldi element have been documented [9–13].

In this paper, we have developed two different Vivaldi antenna arrays for see through dry wall and concrete wall UWB applications utilizing antipodal and tapered slot antennas (TSA) respectively. The configurations of the array element were optimized to have a compact size. The antipodal antenna array operates at 8–12 GHz for high resolution imaging through dry-walls, while the TSA array operates at a lower band (2–4 GHz) with a similar size, however, both have more than 12 dBi gain at the respective operating band. Details of the developed Vivaldi antennas, Wilkinson power dividers [14, 15], the sub and full Vivaldi antenna arrays, their simulation and experimental results will be presented in this paper.

2. VIVALDI ANTENNA ELEMENTS

2.1. Antipodal Vivaldi Element

In this design Antipodal Vivaldi antenna element [16] and Wilkinson divider are used to achieve a bandwidth of 8 to 12 GHz. The main advantage of this element over regular Vivaldi element is that very wideband performance can be achieved using the antipodal tapered profile with its inherently simple wideband transition from microstrip line to parallel-strips. Both simulated and measured results are presented.

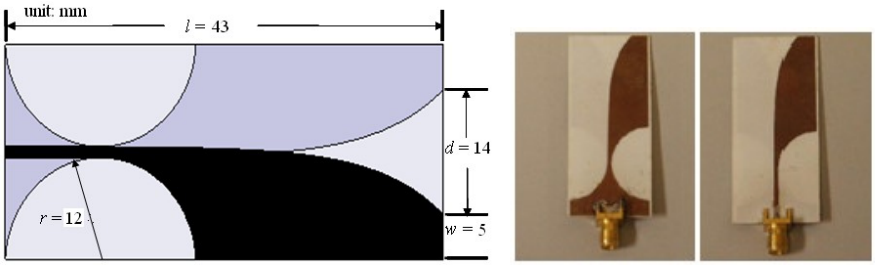

Figure 1. Designed antipodal Vivaldi antenna.

The design parameters and manufactured Antipodal element are shown in Figure 1. Exponential tapered profile is a common shape to obtain a relatively wide impedance bandwidth. The manufactured antenna was fabricated on a 20-mil Roger 4003C material with a relative dielectric constant of 3.4 and a loss tangent of 0.0027. The top and bottom layers show the exponential taper profile [17] which

is defined by the opening rate R and the two points $P_1(x_1, y_1)$ and $P_2(x_2, y_2)$ (use the first and the last points of the exponential taper)

$$y = c_1 e^{Rx} + c_2 \tag{1}$$

where

$$\begin{aligned} c_1 &= \frac{y_2 - y_1}{e^{Rx_2} - e^{Rx_1}} \\ c_2 &= \frac{y_1 e^{Rx_2} - y_2 e^{Rx_1}}{e^{Rx_2} - e^{Rx_1}} \end{aligned} \tag{2}$$

Given the highest frequency of operation (f_H), the width $d+2w$ of the antipodal vivaldi antenna should satisfy Equation (3) to circumvent any grating lobes for the Vivaldi array.

$$d + 2w < \frac{c}{f_H \sqrt{\varepsilon_e}} \tag{3}$$

where ε_e is the effective dielectric constant. In addition, the antenna is fed by a microstrip through a stripline transition as shown in Figure 1. The simulated far field radiation patterns of this element at a center frequency of 10 GHz are illustrated in Figure 2. The element has $\sim 70^\circ$ 3 dB beamwidth with a 5 dB gain.

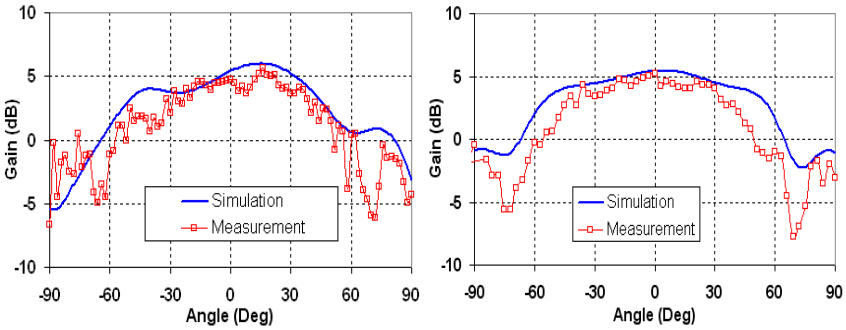

(a) E-plane (b) H-plane

Figure 2. Radiation pattern of single element at 10 GHz.

2.2. Tapered Slot Antenna Element

For the 2–4 GHz operation, a tapered slot antenna design was developed. The design parameters of the proposed TSA and the fabricated parts are shown in Figures 3 and 4 respectively. The

manufactured TSA was fabricated on Rogers RT5880 material with a relative dielectric constant of 2.2, thickness of 0.062" and a loss tangent of 0.0009. The top layer shows the microstrip line and the series radial stub used for feeding the tapered slot antenna. The bottom layer indicates the exponential taper profile which is defined by the opening rate R and was similarly determined by the first and last points as in the case of the antipodal Vivaldi antenna. Given the highest frequency of operation (f_H), the width W of the tapered slot antenna here should also satisfy Equation (3) to circumvent the grating lobes of the Vivaldi array.

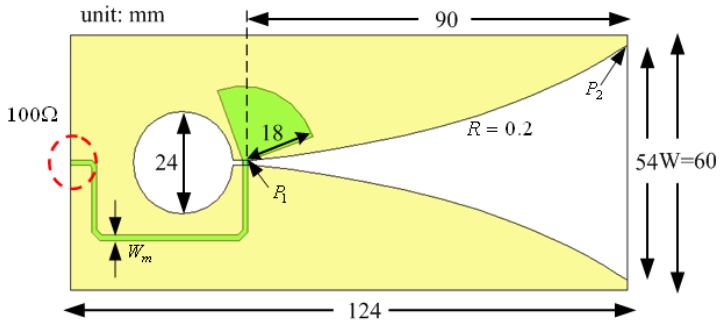

Figure 3. Configurations of the proposed TSA.

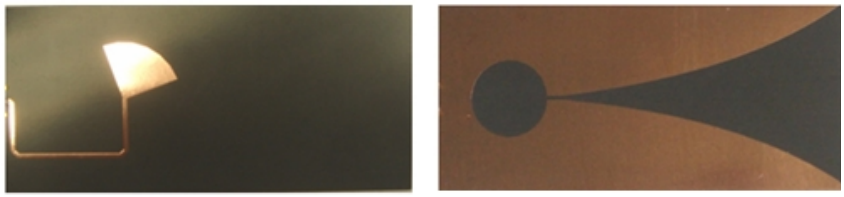

Figure 4. Top and bottom view of the manufactured TSA.

In addition, the TSA has been designed for a 100 Ω instead of 50 Ω. Therefore, we defined the width of the microstrip line feeder W_m to give the characteristic impedance of 100 Ω, and followed similar design steps as Shin et al. [18] to achieve a wideband performance. After defining the parameters cited above, all other parameters are optimized with Ansoft High Frequency Structure Simulator (HFSS) to get both the compact size and good performance at the operating band.

3. DESIGN OF WIDEBAND WILKINSON POWER DIVIDERS

A wideband Wilkinson power divider [14, 19]is needed to feed the Vivaldi array. A 3-section Wilkinson power divider [14], which provides signals with balanced amplitudes and phases from the output ports, is selected to compose the 16-way feed network for the antipodal Vivaldi antenna array, and 8-way for the TSA array. The manufactured 2-way wideband Wilkinson power divider for the TSA is shown in Figure 5. The input and the two output ports are matched at a characteristic impedance of 100 Ω so that the power divider can be directly connected with the tapered slot antennas. Figure 6 indicates the simulated return loss and insertion loss of the power divider. In the operating band from 2 to 4 GHz, the return loss is lower than −15 dB and output ports have almost equal power level with insertion loss of −3.3 dB and ±0.2 dB fluctuation.

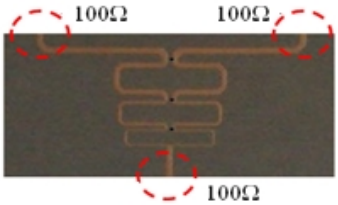

Figure 5. Two-way Wilkinson Power Divider for 2–4 GHz application.

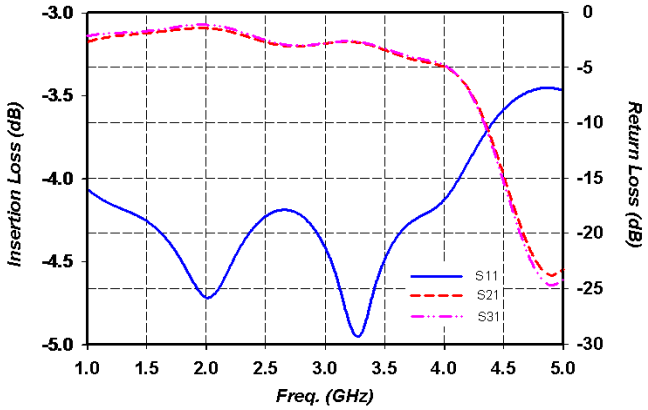

Figure 6. Simulated return loss and insertion loss of 2–4 GHz power divider (normalized to 100 Ω).

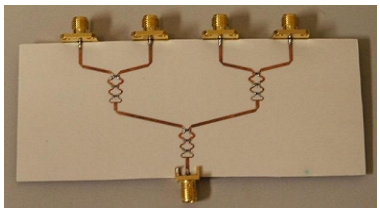

Figure 7. Manufactured 1 to 4 Wilkinson divider for 8–14 GHz application.

Similarly, a divider is needed here for feeding our 16-element array. Again, the 3-section Wilkinson divider [14] is chosen to compose the 16-way binary-tree divider. A 1 to 4 Wilkinson divider was designed and built to test the performance, shown in Figure 7. The predicted transmission and reflection performance of a 4-way divider is shown in Figure 8(a). Insertion loss of each path is about -7 dB with $+1$ dB to -1 dB fluctuation — which corresponds to an extra 1 dB loss due to the ohmic losses. Meanwhile, the return loss at input port is better than -10 dB from 8 to 14 GHz. Measured return and insertion loss of the 1:4 feed divider are shown in Figures 8(b) and (c). The return loss of each port is below -10 dB from 8 to 14 GHz, and both are in good agreement with the predicted results. Measured results of other ports are not plotted out in Figure 8 but they follow the same patterns as that shown by $S21$ and $S11$. Thus, it is anticipated to have about 3–4 dB overall loss for the three stage dividers; i.e., the 1:16 way power divider.

4. DESIGN OF VIVALDI SUB-ARRAYS

4.1. Design of a 16-Element Antipodal Vivaldi Sub-array

Sixteen antipodal elements are combined through a Wilkinson power divider to form a sub-array with a fixed beam. The previously discussed 3-section Wilkinson divider is chosen to compose the 16-way divider, and provides signals with equal amplitudes and phases over the 8–12 GHz bandwidth. The top and bottom layers of the fabricated 16-element subarray are shown in Figure 9. The element spacing is equal to the width of an element, which is $(d + 2w) = 24$ mm (0.946 in) based on simple grating lobe analysis indicated below. The overall size of this sub-array is 178 mm $\times$ 406 mm (7in $\times$ 16 in). To ensure no

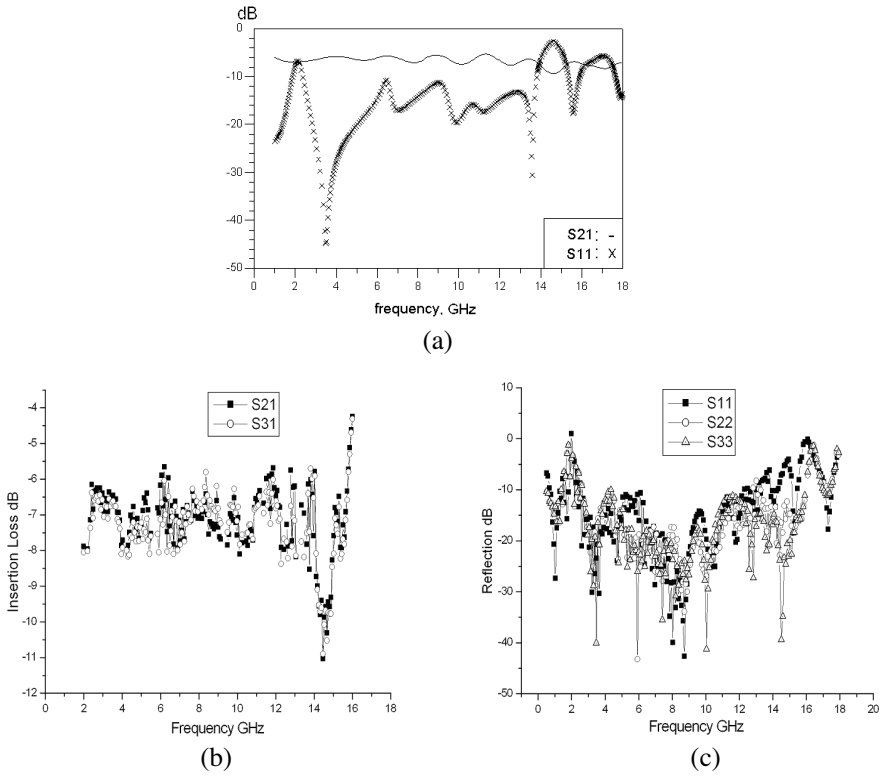

Figure 8. (a) Simulated return loss and transmission, (b) Measured insertion loss and (c) Reflection of 4-way Wilkinson array.

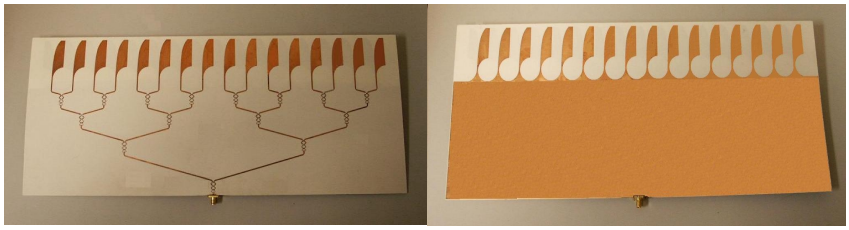

Figure 9. Top and bottom views of the manufactured 1×16 Vivaldi array.

grating lobes, the following condition should be satisfied [20],

$$(d + 2w) < \frac{\lambda}{1 + |\cos \phi_0|} \tag{4}$$

where $(d + 2w)$ is the element spacing, λ is the wavelength at the operating frequency, and ϕ_0 is the main beam angle. For this 16-element sub-array, only the broadside needs to be considered. At broadside, $\phi_0 = -90$ degree, this reduces the earlier condition $(d + 2w) < \lambda$. This subarray spacing, 24 mm, is slightly smaller than λ_0 up to 12 GHz, which predicts a grating lobe beyond 12 GHz, or higher sidelobe levels at higher operating frequency. The main beamwidth of an array is given by the following formula [20],

$$\Delta\phi_{3\,\mathrm{dB}} = \frac{0.886}{\sin\phi_0}\frac{\lambda}{Nd}, \tag{5}$$

which predicts that around 10 GHz this subarray has 4 degrees 3 dB-beamwidth in the E-plane.

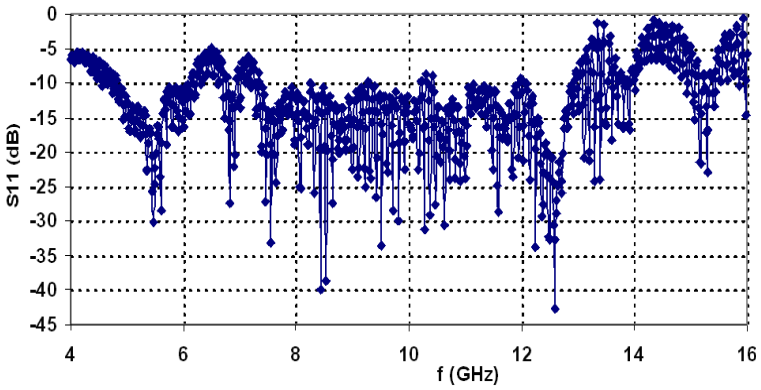

Figure 10. Measured return loss of the 1×16 array.

The measured return loss of the Vivaldi sub-array shows a good match from 8–12 GHz, as shown in Figure 10. The measured pattern of the subarray is shown in Figure 11. The subarray has almost constant pattern within the operating frequency range. The measured gain varies from 13 dB to 14 dB, with a 1 dB fluctuation. The subarray of the 16 elements should ideally have a 17 dB gain, and the 3 dB gain drop is due to the loss of the Wilkinson network as previously indicated. The closest visible sidelobe occurs at 80° at 12 GHz in the E plane; and the 3-dB beamwidth is about 4° in the E-plane and 70° in the H-plane. These measured results match the theoretical values predicted by Equation (5).

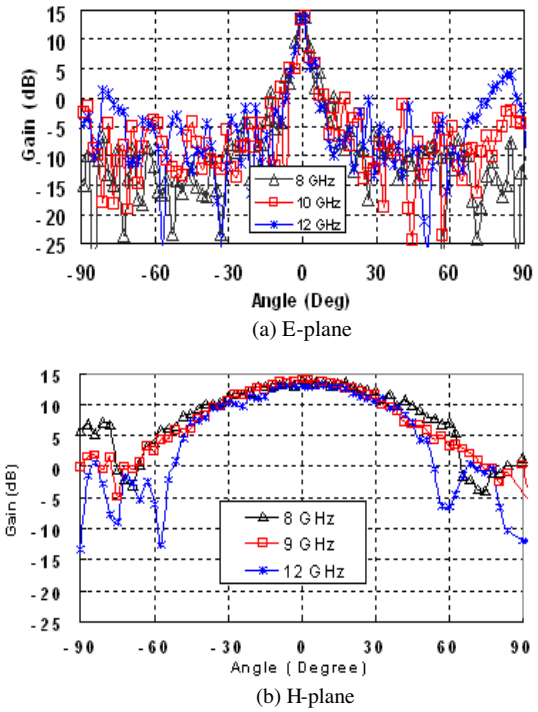

(a) E-plane

(b) H-plane

Figure 11. Measured antipodal sub-array pattern.

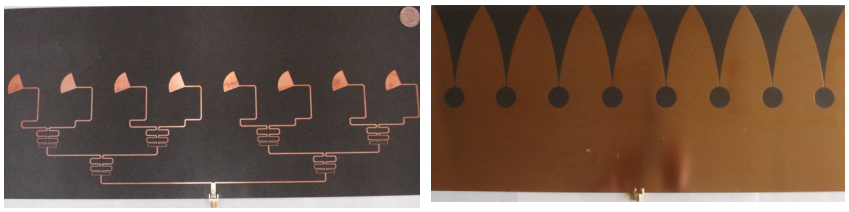

(a) Top view (b) Bottom view

Figure 12. Manufactured tapered slot sub-array.

4.2. Design of an 8-Element Tapered Slot Sub-array

An eight-element tapered slot array was fabricated to operate over the 2–4 GHz range. It was printed on Rogers RT5880 material. Figure 12 demonstrates the top layer and bottom layer of the manufactured array, where eight single Vivaldi antennas were fed by cascaded Wilkinson power divider network. As shown in Figures 3 and 5, TSA and binary

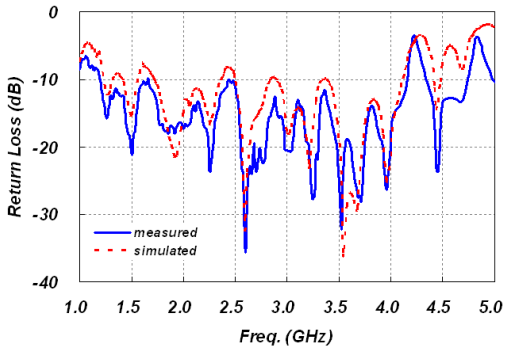

Figure 13. Measured and simulated return loss (normalized to 50 Ω).

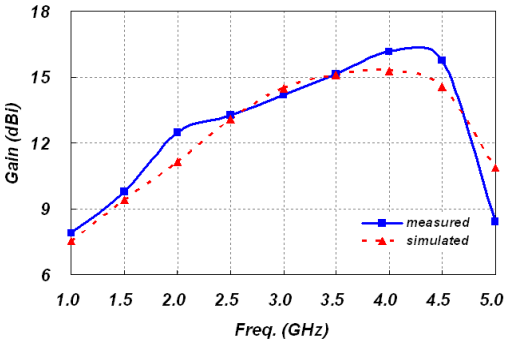

Figure 14. Measured and simulated Gain vs. frequency.

Wilkinson power divider are both matched to 100 Ω. At the feeding port of the 8-element array, two Wilkinson power dividers were shunted together to make the array matched to 50 Ω. The spacing between two adjacent elements W, indicated in Figure 3, is $0.8\lambda_0$ at the highest operating frequency 4 GHz to suppress grating lobes. The overall size of the array is 480 mm × 210 mm (8in × 19in). Measured and simulated results of the Vivaldi antenna array are shown in Figures 13–15. Measured results in Figure 13 indicate that the array can operate from 1.2 to 4.2 GHz with a return loss of lower than −10 dB. A gain of more than 12 dBi is sustained over the frequency range 2 to 4 GHz, as shown in Figure 14. Figure 15 demonstrates the measured radiation pattern of the Vivaldi antenna array at 2, 3 and 4 GHz, which shows that the side lobes are 15 dB lower than the main beam in the azimuth plane.

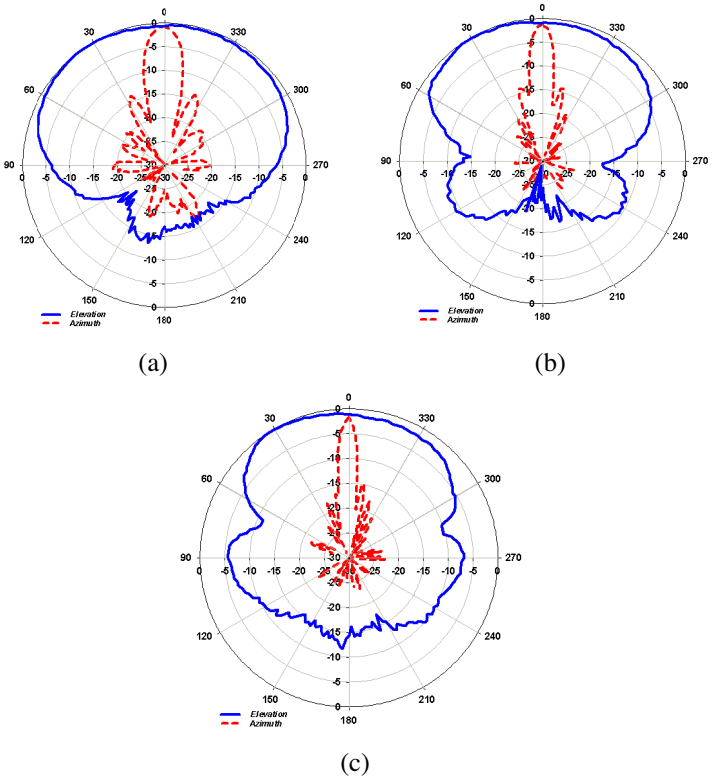

Figure 15. Measured radiation pattern: (a) 2 GHz, (b) 3 GHz, (c) 4 GHz.

The simulated gain shown in Figure 14 is higher than the measurement. There are two factors that contribute to the higher simulation result. Firstly only one prototyped antenna covering 2–4 GHz was fabricated in our experiment and hence a wide band flared horn was used for measurements, which is typically difficult to accurately carry out such gain measurements over a 1:4 frequency range. In general it is preferred to have identical antennas for better measurements. It is believed that $+/-1$ dB variation can be expected from our measurement. Secondly, HFSS was used to simulate the 8-element 2–4 GHz array. Due to its large size, it took 20 hours to run a case for a PC with a 2.2 GHz Core2 Duo CPU and 3.0 GB RAM, and it is hard to get very accurate simulation for such big arrays. In other words, the agreement between measured and simulated results is adequate for such big arrays.

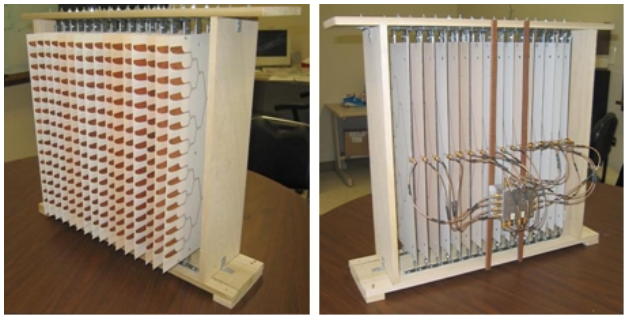

Figure 16. Manufactured 16×16 Vivaldi array.

5. A FULL ARRAY EXAMPLE

5.1. Design of the Full Array

A full array with sixteen 16-element sub-arrays was built for 8–12 GHz operation and is shown in Figure 16. This full array has a fixed elevation beam pattern (E plane) shown in Figure 11(a), and can be synthetically steered in the azimuth plane (H plane). The sub-array spacing is set to 2.4 cm, which is 0.8λ at 10 GHz for suppressing grating lobes over the scanning angle from -30° to 30°. The synthesized azimuth (H plane) 3-dB main beamwidth is around 4° at broadside, according to Equation (5) in Section 5. Because of the presence of $\sin\phi_0$ in the denominator, the beamwidth will get broader as the array is synthetically steered from broadside to near endfire. For a fixed operating frequency range, one can either increase the inter-element spacing d or the number of array elements N to decrease the main beamwidth and improve array directivity. However, increasing N will make the array larger and more complicated to fabricate; increasing d will cause grating lobes and would limit the viewing angle. Depending on different applications requirements, a trade-off must be made between the array performance such as the main beamwidth and steering range, and the array design degrees of freedom such as the inter-element spacing and the number of elements [21].

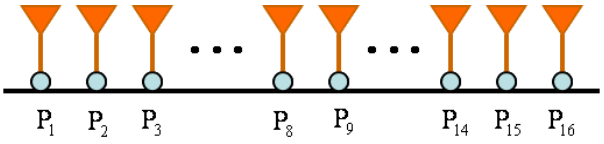

Figure 17. Array configuration for mutual coupling measurement.

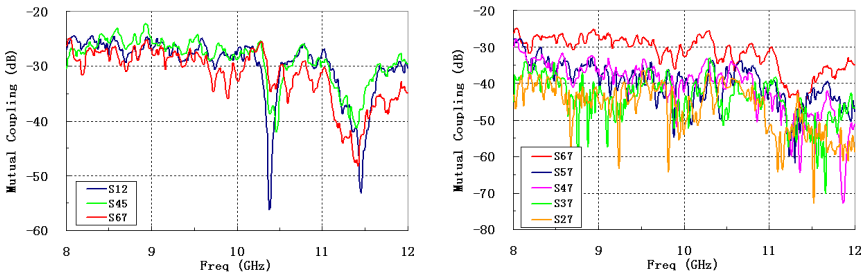

Figure 18. Mutual coupling between 16 sub-arrays.

The above antipodal Vivaldi array is built for Synthetic array operation where only one single antenna is used at a time. Hence, mutual coupling due to the presence of the neighboring elements must be minimized. In our implementation with a physical spacing of 2.4 cm, the coupling between these 16 sub-array elements is less than −23 dB as shown in Figure 18. Mutual coupling effects on the radiating element patterns have been also investigated as indicated in Figure 19, where the radiation pattern was measured first for one sub-array (the central one), then compared to those of adding N sub-arrays at both sides of the central one. In Figure 19, $N = 0$ means there is no neighboring sub-array next to the central one, $N = 1$ means adding one terminated sub-array at both sides of the central sub-array, and so on. The differences between these various radiation patterns are not significant and for all practical reasons they have been assumed constant in our SAR code implementation.

The measurement indicates that the assumption that all sub-arrays are adequately independent of each other is a good approximation; otherwise extensive calculations are required to account for the radiation pattern variation for different sub-arrays in the SAR code implementation [22–25]. Wider spacing between the elements should reduce the mutual coupling between the elements, but it could cause unwanted grating lobes.

5.2. Design of a UWB SP16T Switch

A Single Pole 16 Throw (SP16T) switch was designed to automate the full array. The SP16T switch is comprised of 15 Single Pole Double Throw (SPDT) switch units, utilizing a binary tree structure, shown in Figure 20. The used SPDT is Hittite HMC347LP3, a Monolithic Microwave Integrated Circuit (MMIC) [26] with 1.7-dB insertion loss, 40-dB isolation, and DC-14 GHz range. The binary tree has 4 layers, and each layer has $2^{(n-1)}$ SPDT units.

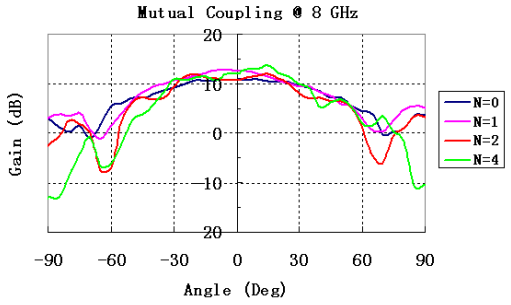

(a) @ 8GHz

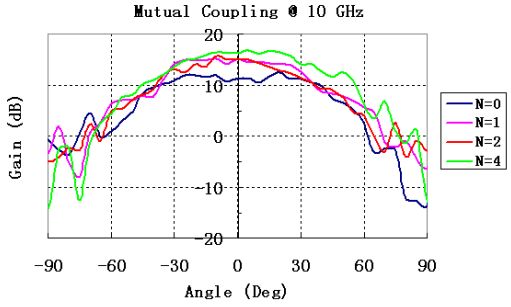

(b) @ 9GHz

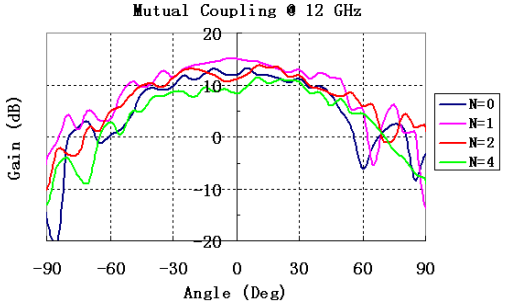

(c) @ 10GHz

Figure 19. Radiation pattern considering mutual coupling effects.

The MMIC board is made of 20-mil Roger 4003C substrate and placed in a customized alumni package (Figure 21(a)). The switch driver (Figure 21(b)) is comprised of 74HC04 chips and utilizes 4:16 decoder topology. The driver input is a 4-bit TTL word providing 16 logic states, from "0000" to "1111", each of which turns on the corresponding channel. More details of the switch and driver circuit

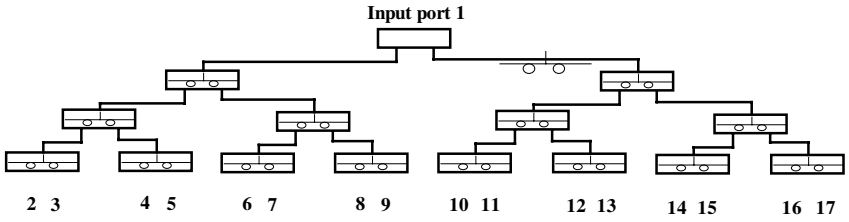

Figure 20. SP16T binary tree.

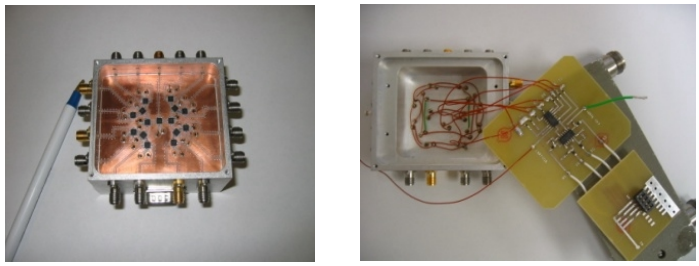

(a) (b)

Figure 21. (a) SP16T package; (b) Driver circuit.

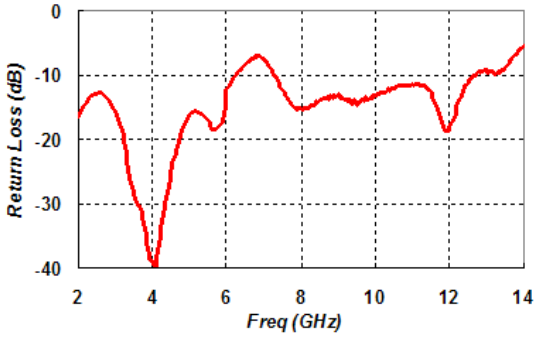

Figure 22. Typical measured return loss of one of 16 channels.

design can be found in [27]. The measured return loss in Figure 22 indicates that the designed switch covers both higher frequency band of 8–12 GHz and lower band of 2–4 GHz. The measurement also shows that the SP16T has considerably high insertion loss of 8-dB at higher frequency band, in Figure 23. The high loss results from the multiple-layer binary tree structure and the 1.7 dB loss of each SPDT element. However, significant performance improvement and design complexity

reduction can be achieved upon utilizing the recently available Hittite HMC344 SP4T switch.

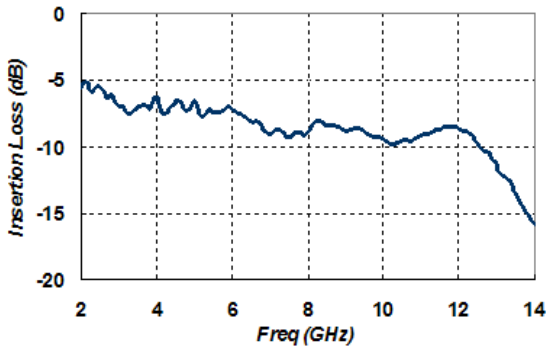

Figure 23. Typical measured insertion loss of one of 16 channels.

6. CONCLUSIONS

In this paper, two designs for Vivaldi antenna arrays suitable for see through wall applications were presented. The tapered slot Vivaldi antenna array was developed to be part of the see through concrete wall detection. While, the antipodal Vivaldi antenna array was developed for higher resolution images through low loss walls like dry-walls. The antennas and wideband Wilkinson power dividers were utilized to compose the array and were optimized to get a compact size. The measured results of the return loss, gain and radiation patterns demonstrated good performances of the Vivaldi arrays. An example of the full array comprised of sixteen 16-element sub-arrays was introduced. The full array has adequate decoupling of 23 dB or higher between the neighboring sub-arrays to minimize mutual coupling effects. The design of an ultra-wideband SP16T switch to automate the full array was discussed.

ACKNOWLEDGMENT

The authors would like to thank Rogers Company for donating the Rogers RO4003 and RT5880 substrates.

REFERENCES

1. Wang, F.-J. and J.-S. Zhang, "Time domain characteristics of a double-printed UWB bipole antenna," *Progress In Electromagnetics Research Letters*, Vol. 3, 161–168, 2008.
2. Mehdipour, A., K. M-Aghdam, and and R. Faraji-Dana, "Completed dispersion analysis of Vivaldi antenna for ultra wideband applications," *Progress In Electromagnetics Research*, PIER 77, 85–96, 2007.
3. Gibson, P. J., "The Vivaldi aerial," *Proc. 9th Eur. Microwave Conf.*, June 1979.
4. Janaswamy, R. and D. H. Schaubert, "Analysis of the tapered slot antenna," *IEEE Trans. Antennas Propagat.*, Vol. AP-35, 1058–1064, Sept. 1987.
5. Stockbroeckx, B. and A. V. Vorst, "Copolar and cross-polar radiation of Vivaldi antenna on dielectric substrate," *IEEE Trans. Antennas Propagat.*, Vol. 48, 19–25, Jan. 2000.
6. Greenberg, M. C., L. Virga, and C. L. Hammond, "Performance characteristics of the dual exponentially tapered slot antenna for wireless communication application," *IEEE Trans. on Vehicular Technology*, Vol. 52, 305–310, Mar. 2003.
7. Shafieha, J. H., J. Noorinia, and Ch. Ghobadi, "Probing the feed line parameters in Vivaldi notch antennas," *Progress In Electromagnetics Research B*, Vol. 1, 237–252, 2008.
8. Rajabi, M., M. Mohammadirad, and N. Komjani, "Simulation of Ultra wideband microstrip antenna using EPML-TLM," *Progress In Electromagnetics Research B*, Vol. 2, 115–124, 2008.
9. Greenberg, M. C., L. Virga, and C. L. Hammond, "Performance characteristics of the dual exponentially tapered slot antenna for wireless communication application," *IEEE Trans. on Vehicular Technology*, Vol. 52, 305–310, Mar. 2003.
10. Kim, S. G. and K. Chang, "Ultra wideband 8 to 40 GHz beam scanning phased array using antipodal exponentially-tapered slot antennas," *IEEE MTT-S Digest*, 1757–1760, 2004.
11. Ehud Gazit, E., "Improved design of the Vivaldi antenna," *Proceeding Inst. Elect. Eng.*, pt. H, Vol. 135, No. 2, 89–92, 1988.
12. Schaubert, D. H. and T.-H. Choi, "Wideband Vivaldi arrays for large aperture antennas," *Perspectives on Radio Astronomy: Technologies for Large Antenna Array*, 49–58, 1999.
13. Langley, J. D. S., P. S. Hall, and P. Newham, "Balanced antipodal Vivaldi antenna for wide bandwidth phased arrays," *Proc. IEEE*

Antennas Propagation, Vol. 143, 97–102, Apr. 1996.

14. Cohn, S. B., "A class of broadband three-port TEM-mode hybrids," *IEEE Trans. Microwave Theory & Techniques*, Vol. MTT-16, No. 2, 110–116, Feb. 1968.
15. Guo, Y. and R. Xu, "Ultra-wideband power splitting/combing technique using zero-degree left-handed transmission lines," *J. of Electromagn. Waves and Appl.*, Vol. 21, No. 8, 1109–1118, 2007.
16. Ehud Gazit, E., "Improved design of the Vivaldi antenna," *Proc. Inst. Elect. Eng.*, pt. H, Vol. 135, No. 2, 89–92, Apr. 1988.
17. Greenberg, M. C., L. Virga, and C. L. Hammond, "Performance characteristics of the dual exponentially tapered slot antenna for wireless communication application," *IEEE Trans. on Vehicular Technology*, Vol. 52, 305–310, Mar. 2003.
18. Shin, J. and D. H. Schaubert, "A parameter study of stripline-fed Vivaldi notch-antenna arrays," *IEEE Trans. on Antenna and Propagation*, Vol. 47, No. 5, 879–886, May 1999.
19. Shamsinejad, S., M. Soleimani, and N. Komjani, "Novel miniaturized Wilkinson power divider for 3G mobile receivers," *Progress In Electromagnetics Research Letters*, Vol. 3, 9–16, 2008.
20. Orfanidis, S. J., *Electromagnetic Waves and Antennas*, Rutgers University, Feb. 2008.
21. Chan, Y. K. and V. C. Koo, "An introduction to synthetic aperture radar (SAR)," *Progress In Electromagnetics Research B*, Vol. 2, 27–60, 2008.
22. Zhu, Y.-Z., Y.-J. Xie, Z.-Y. Lei, and T. Dang, "A novel method of mutual coupling matching array antenna design," *J. of Electromagn. Waves and Appl.*, Vol. 21, No. 8, 1013–1024, 2007.
23. Tian, Y., Y.-H. Zhang, and Y. Fan, "The analysis of mutual coupling between paraboloid antennas," *J. of Electromagn. Waves and Appl.*, Vol. 21, No. 9, 1191–1203, 2007.
24. Liang, C.-H., L. Li, and X.-J. Dang, "Inequality condition for grating lobes of planar phased array," *Progress In Electromagnetics Research B*, Vol. 4, 101–113, 2008.
25. Vescovo, R., "Beam scanning with null and excitation constraints for linear arrays of antennas," *J. of Electromagn. Waves and Appl.*, Vol. 21, No. 2, 267–277, 2007.
26. Chan, Y. K. and S. Y. Lim, "Synthetic aperture radar signal generation," *Progress In Electromagnetics Research B*, Vol. 1, 269–290, 2008.
27. HMC347LP3 Data Sheet, v03.0604, Hittite Microwave Corporation.